Journal of Materials Chemistry B

PAPER

View Article Online
View Journal | View Issue

Cite this: J. Mater. Chem. B, 2019, 7, 6972

A mimotope peptide-based dual-signal readout competitive enzyme-linked immunoassay for non-toxic detection of zearalenone†

Yanjie Chen,[a] Shupei Zhang,[b] Zhensheng Hong,[a] Yanyu Lin[c] and Hong Dai *[ab]

Received 11th June 2019,
Accepted 3rd October 2019

DOI: 10.1039/c9tb01167f

rsc.li/materials-b

In this study, a mimotope peptide-based non-toxic photoelectrochemical (PEC) competitive enzyme-linked immunoassay (ELISA) was established for ultrasensitive detection of zearalenone (ZEN) with dual-signal readout. Using the phage display technique (PDT), a mimotope peptide of ZEN could be harvested by selecting a peptide from a phage-display peptide library, which avoided using mycotoxin itself and minimized potential damage to operators. The tyramine-modified rutile TiO_2 mesocrystals (Tyr-RMC) with outstanding PEC properties were utilized as reporter units to label the mimotope peptide. The fabricated peptide@Tyr-RMC probe could anchor on the antibody-modified electrode *via* competitive immune recognition of free target ZEN. When subjected to catalysis of HRP–H_2O_2, the Tyr-RMC composite was deposited at the enzyme reaction site, causing rolling circle extension of the reporter unit chains. By merit of the brilliant signal amplification effect of tyramine signal amplification (TSA), dramatically enhanced photocurrent response and enormously increased electrochemical impedance could be determined. Combining all of these advantages, the developed dual-signal readout non-toxicity immunoassay could effectively decrease environmental interference. Also, the designed dual-signal readout biosensor demonstrated a wide linear range between 10^{-6} and 1 ng mL^{-1} with a low detection limit of 1×10^{-6} ng mL^{-1}, which provides a valuable reference for developing highly efficient, secure and sensitive detection methods and indicates promising applicability in food testing.

1. Introduction

Zearalenone (ZEN) is a common estrogenic mycotoxin that has disruptive effects on hormonal balance; it can cause various diseases, including central precocious puberty, reproduction problems and even spontaneous abortion.[1–3] Usually, ZEN is widely present in human foods, such as flour, tortillas, and corn oil, and it is produced during the grain and storage process.[4,5] Therefore, to date, extensive efforts have been devoted to exploring new methods for sensitive ZEN detection, including fluorescent ELISA,[6] fluorescence,[7] immunochromatography,[8] and fluoroimmunoassays.[9] Although these approaches have indeed realized accurate detection of ZEN, some drawbacks remain to be addressed, including complex pretreatment processes and expensive and bulky instruments. Currently, the photoelectrochemical (PEC) technique has attracted considerable attention as a newly emerging and rapid developing analysis technology due to its merits of high sensitivity, simple instrumentation, and low cost. Despite this, conventional approaches for ZEN monitoring in food usually involve extracting it from contaminated raw feed or finished food, which involves using the mycotoxin itself and may be toxic to manufactures and users.[10] Consequently, it is urgent to propose powerful and reliable methods for non-toxic monitoring of ZEN.

The phage display technique (PDT) is a delicately designed biological technique that functions brilliantly in polypeptide separation. The basic principle of PDT is to utilize a modified phage as a carrier and insert the selected gene fragment into the gene of the phage shell protein. As per this system, the desired peptides are expressed by the modified phages and displayed as components of their surface proteins, which can then be collected and utilized as a target mimic.[11–13] According to previous research, the monoclonal antibody 7G5 (McAb 7G5) with the capacity of recognizing ZEN can be utilized to select for surface peptides from a filamentous phage library. Also, the harvested phage-displayed peptides can be used as mimotope peptides of ZEN (ZMP).[10] Herein, an innovative less-toxic or non-toxic PEC immunosensor was developed simply by utilizing ZMP as a substrate of the probe to undergo a competitive reaction with free target ZEN.

[a] College of Chemistry and Materials, Fujian Normal University, Fuzhou 350108, P. R. China. E-mail: dhong@fjnu.edu.cn; Fax: +86-591-22866135
[b] Fujian Provincial Maternity and Children's Hospital, Affiliated hospital of Fujian Medical University, Fuzhou, Fujian, 350108, China
[c] Ministry of Education Key Laboratory of Analysis and Detection for Food Safety, and Department of Chemistry, Fuzhou University, Fuzhou 350002, P. R. China

† Electronic supplementary information (ESI) available. See DOI: 10.1039/c9tb01167f

In addition to non-toxic detection, versatile photoactive materials and delicate sensing strategies are required to enhance the sensitivity of PEC biosensors. Rutile TiO_2 mesocrystals (RMC) are known as a promising PEC sensing material due to their distinctive features of nontoxicity, high porosity and large specific surface area.[14] Moreover, the particular mesoporous 3D structures in RMC allow multidimensional accepting and scattering of light, thereby exhibiting unique advantages, such as good light-scattering and light-reflecting effects, higher dielectric constants, electric resistance and chemical stability.[15] All of these properties can notably improve PEC performance during measurements. Tyramine signal amplification (TSA) has been substantially applied as an efficient signal amplification strategy in the field of cell and protein analysis due to its simple operation and good amplification effects.[16,17] By virtue of this, a valid rutile TiO_2 mesocrystals-enhanced tyramine signal amplification (RMC-TSA) strategy was developed by employing tyramine-modified RMC (Tyr-RMC) as a reporter molecule to label ZMP. Subject to catalysis of horseradish peroxidase (HRP) and hydrogen peroxide (H_2O_2), the Tyr-RMC composite is deposited at the site of the enzyme reaction, resulting in rolling circle extension of the reporter unit chains.[18,19] Consequently, under illumination, a large number of excited electronics are persistently generated from the RMC chain and injected into the electrode interface, which causes enormously increased photocurrent response. Furthermore, the localized accumulation of reporter units also results in rolling circle amplification of the electrochemical impedance because the semiconductor properties of RMC can greatly inhibit electron transfer. Therefore, benefitting from the superior signal amplification effect of RMC-TSA, a powerful dual-signal readout amplification platform was established which considerately improved the analytical performance of this PEC sensing platform.[20]

Herein, a valid non-toxic dual-signal readout strategy for specific and sensitive detection of ZEN is reported. To fabricate the assay system, as illustrated in Scheme 1, carbon nanohorns (CNHs) and Au nanocones (Au NCs) were coated onto an electrode as a substrate. The Schottky barrier and localized surface plasmonic resonance between the two materials attached to the sensing interface enhanced the conductivity and prolonged the lifetime of electrons.[21,22] On the other hand, inspired by PDT, a ZMP selected from a phage library was employed as a probe substrate, and the Tyr-RMC composite was utilized as a reporter unit to label the ZMP. After peptide@Tyr-RMC was captured on the electrode interface *via* immune recognition, the modified electrode was subsequently catalyzed with HRP–H_2O_2. As a result, the Tyr-RMC composite was deposited at the site of the enzyme reaction, causing rolling circle extension of the reporter unit chains and thereby leading to dramatically enhanced photocurrent response as well as enormously increased electrochemical impedance. Due to its outstanding amplification effects and non-toxic operation, this PEC biosensor demonstrated excellent sensitivity, reliability and safety. Promisingly, the successful fabrication and application of the biosensor can serve as guidance for the rational construction of non-toxic and highly efficient PEC sensing platforms.

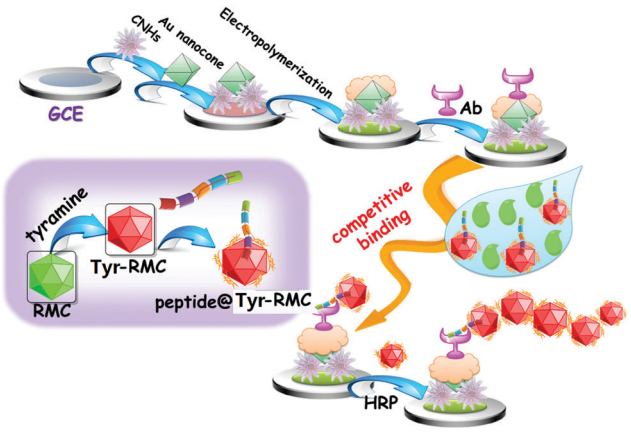

Scheme 1 Illustration of the construction process of the PEC biosensor.

2. Experimental

2.1 Reagents

Zearalenone (ZEA) standard and ZEN antibody were acquired from Wuxi Biosensor Technology Co., Ltd (Jiangsu, China). The mimotope peptide of ZEN (amino acid sequence: DAVILLM) was purchased from Dangang Biotechnology Co., Ltd (Hangzhou, China). Aflatoxin B1 (AFB1), deoxynivalenol (DON), $HAuCl_4{\cdot}3H_2O$, $H_2PtCl_6{\cdot}6H_2O$ and $NaBH_4$ were all purchased from Sigma-Aldrich Co. Ltd (Shanghai, China). HRP and tyramine were received from Sinopharm Chem. Re. Co., Ltd (Shanghai, China). Sodium dodecylbenzene sulfonate (SDBS), titanium(IV) isopropoxide (TIP), mercaptoethylamine (MEA), 1-ethyl-3-(3-(dimethylamino)propyl)-carbodiimide (EDC), *N*-hydroxysuccinimide (NHS), glycine (Gly) and trichloroacetic acid were all purchased from Aladdin Co. Ltd (Shanghai, China). Cetyltrimethylammonium bromide (CTAB) and bovine serum albumin (BSA) were obtained from Solarbio Science & Technology Co., Ltd (Beijing, China). The soybean sauce sample was purchased from Hai-Tian Food Co., Ltd (Foshan, China). Other reagents purchased from Sinopham Chemical Reagent Co. (Shanghai, China) were analytical grade and were utilized without further treatment for the following experiments. The phosphate buffer solution (PBS) was prepared by mixing stock solutions of 0.1 M NaH_2PO_4 and 0.1 M Na_2HPO_4 as the supporting electrolyte to adjust the pH value. The EDC/NHS solution was prepared by mixing 20 mM EDC and 10 mM NHS with a volume ratio of 4 : 1. All ultrapure water (18.2 MΩ cm^{-1} at 25 °C) for the experiments was purified with a Milli-Q Advantage water treatment system.

2.2 Apparatus

PEC measurements were performed with a homemade PEC system. Open circuit potential–time (OCP), linear sweep voltammetry (LSV), cyclic voltammetry (CV), amperometric *I–t* curve studies and electrochemical impedance spectroscopy (EIS) were performed on a CHI 760C electrochemical workstation (Shanghai Chenghua Instrument Co., China) with a conventional three-electrode system: Ag/AgCl electrode (sat. KCl) was used as the reference electrode,

modified GCE (Φ = 3 mm) was used as the working electrode and a platinum wire was used as the auxiliary electrode. The electrochemical impedance measurements were determined in a mixed solution of 5.0 mM $K_3[Fe(CN)_6]/K_4[Fe(CN)_6]$ (1 : 1) containing 0.5 M KCl under an applied potential of 0.199 V. All the PEC measurements were carried out under an applied potential of 0.2 V in PBS (pH 7.0). The pH measurements were performed on a PHS-3C exact digital pH meter (Leici Co. Ltd, Shanghai, China), which was calibrated with standard pH buffer solutions. The excitation source of homogeneous light (395 nm) was filtered from a xenon lamp (86 mW cm^{-2}, Beijing, China) by a monochromator before use. Scanning electron microscopy (SEM, S4800 instrument) was utilized for structural characterization of the rutile TiO_2 mesocrystals. Transmission electron microscopy (TEM, FEI F20 STWIN) and high-resolution TEM (HRTEM) analysis of the prepared products were performed on a JEOL-2100 transmission electron microscope. X-ray diffraction (XRD) patterns were recorded on a PANalytical X'Pert spectrometer using Co Kα radiation (l = 1.78897 Å), and the data were changed to Cu Kα data. Ultraviolet visible absorption spectra were recorded on a UV-3600 UV spectrophotometer (Shimadzu Ltd, Japan).

2.3 Synthesis of rutile TiO_2 mesocrystals

Typically, 1 g sodium dodecyl benzene sulfonate (SDBS) was dissolved in 50 mL 2.2 M HNO_3 solution at room temperature and stirred for 3 min. Following that, 1 mL titanium(IV) isopropoxide (TIP) was added, and the mixture was maintained at 80 °C for 48 h under stirring. The final products were collected by centrifuging the mixture and washing the sediment with distilled water and ethanol 4 to 5 times. After that, the product was dried overnight at 60 °C followed by calcination at 400 °C for 1 h in air to remove the residual organics to harvest pure rutile TiO_2 mesocrystals (RMC).[23]

2.4 Synthesis of peptide@Tyr-RMC conjugate

Initially, 100 μL of 3 mg mL^{-1} RMC suspension and 200 μL of 5 mg mL^{-1} tyramine solution were prepared and mixed together under sonication for 30 minutes. The tyramine was coated on the RMC *via* hydrogen bonds between the hydroxyl groups of tyramine and Ti-OH on the RMC surface.[32] Next, the mixture solution was centrifuged for 10 min at 6000 rpm to remove physically absorbed tyramine. After that, the sediment was dispersed with 200 μL PBS (pH 7.4) to obtain the Tyr-RMC composite solution. Additionally, 50 μL of 0.5 mg mL^{-1} ZMP was treated with 10 μL of EDC/NHS for 2 h under shaking at room temperature; then, it was added to the Tyr-RMC composite solution prepared above, and the mixture was stirred for 12 hours. The ZMP was connected to Tyr-RMC through the classic EDC/NHS coupling reaction between the amine ($-NH_2$) groups on tyramine and the carboxyl (–COOH) groups of the mimotope peptide. In this process, EDC was used as the coupling agent to react with the carboxyl groups and form an amine-reactive *O*-acylisourea intermediate which was unstable in aqueous solution. Meanwhile, NHS as a stabilizer could react with the *O*-acylisourea intermediate to form the more stable succinimidyl ester intermediate.[33,34] Finally, the peptide@Tyr-RMC was purified by centrifugation (6000 rpm) for 10 min to remove the physically absorbed peptide and collect the sediment. The final product was dissolved with 200 μL PBS (pH 7.4) and stored at 4 °C for use.

2.5 Construction of the PEC biosensor and ZEN detection

Specifically, as shown in Scheme 1, firstly, 3 μL of 3 mg mL^{-1} CNHs suspension was dropped on bare GCE and dried under an infrared lamp. Next, 4 μL of MEA-functionalized Au NCs was dropped onto the electrode, followed by drying the prepared electrode in an oven for 3 min and cooling to room temperature. In succession, the modified electrode was immersed in PBS (pH 7.0) containing 1 mM Gly and scanned with a rate of 0.1 V s^{-1} in the potential window between −0.5 and −1.8 V for 25 cycles to obtain the GCE/CNHs/AuNCs/poly(Gly) electrode. After electrodeposition of poly(Gly), 3 μL of EDC/NHS was also added to activate the carboxyl groups on poly(Gly). Finally, 3 μL of 1 mg mL^{-1} ZEN antibody was dropped onto the electrode, and it was incubated at 4 °C for 50 min; the ZEN antibody was anchored on the electrode *via* the classic EDC/NHS coupling reaction between the amine ($-NH_2$) groups on the antibody and the carboxyl (–COOH) groups on poly(Gly).[39] Following that, the excess ZEN antibody was removed by washing with PBS (pH 7.4), and the electrode was dipped into 1.0 wt% BSA for 30 min to mask the non-specific sites. Therefore, the GCE/CNHs/Au NCs/poly(Gly)/Ab electrode was successfully fabricated after washing thoroughly with PBS (pH 7.4). To perform the assay, the prepared electrode was immersed in a mixed solution of ZEN standard and peptide@Tyr-RMC conjugate to facilitate the competitive assay. Finally, the resulting electrode was treated with 1 mg mL^{-1} HRP (in 2 mM H_2O_2 solution) for 15 min; the Tyr-RMC composite was deposited at the site of the enzyme reaction, leading to rolling circle extension of the reporter unit chains.[36–38] For the photocurrent measurement, the resulting electrode was immersed in PBS (pH 7.0) at room temperature with switchable light excitation under an applied potential of 0.2 V. Also, the electrochemical impedance measurements were performed in a mixed solution of 5.0 mM $K_3[Fe(CN)_6]/K_4[Fe(CN)_6]$ (1 : 1) containing 0.5 M KCl under an applied potential of 0.199 V.

2.6 Analysis of soybean sauce samples

In brief, 10 mL of real soybean sauce sample was treated with 1.0 mL 0.2 g mL^{-1} trichloroacetic acid for 6 h to completely precipitate the impurities in the solution. Subsequently, the harvested sample was purified by centrifuging at a rate of 6000 rpm for 10 min to remove the impurities. The supernatant was diluted 10 times and spiked with 0.1, 0.01 and 0.001 ng mL^{-1} ZEN standard to establish a recovery assay by photocurrent measurement.

3. Results and discussion

3.1 The morphologies of RMC and the Au NCs

The morphologies of RMC and the Au NCs were characterized by SEM and TEM images. As revealed in Fig. 1A, RMC consisted of numerous regular quasi-square nanoparticles with uniform

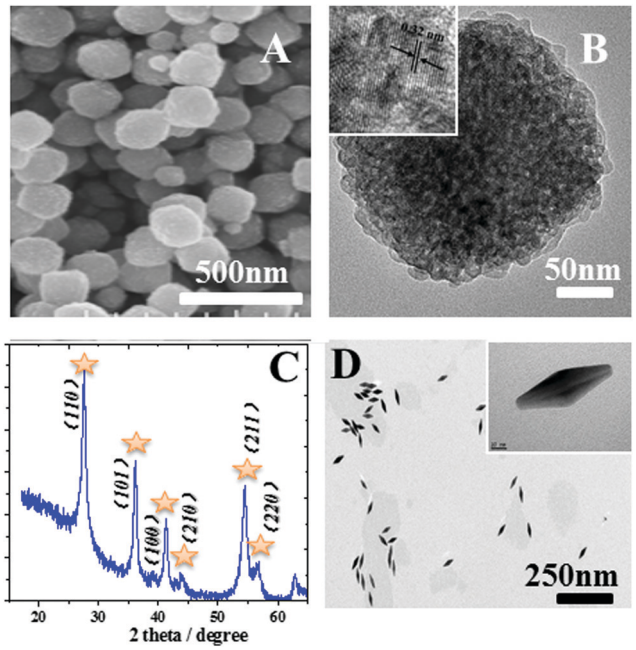

Fig. 1 (A) SEM images, (B) TEM images and (C) XRD pattern of RMC; (D) TEM images of the Au NCs. The inset in (B) shows a HRTEM image of RMC.

sizes. The TEM image in Fig. 1B exhibits that RMC had a rough surface and was composed of tiny nanoparticles with diameters of about 200 nm. The HRTEM image in Fig. 1B exhibits clear lattice fringes with an interplanar spacing of 0.32 nm, which corresponds to the unique (110) plane of rutile TiO_2. In order to further investigate the crystalline structure of RMC, the XRD results are shown in Fig. 1C; the diffraction peaks of the (110), (101), (100), (210), (211), and (220) planes can all be satisfactorily indexed to rutile TiO_2, which confirms the successful synthesis of RMC.[23,24] Fig. 1D displays TEM images of the Au NCs; it is clearly shown that the Au NCs were composed of tiny nanoparticles with irregular structures and were well dispersed. The insert in Fig. 1D reveals the approximate spinning cone structure of the Au NCs with lengths of about 15 nm and widths of about 50 nm.

3.2 PEC behavior of Tyr-RMC

With the aim of investigating the PEC performance of RMC and Tyr-RMC, a series of PEC measurements were carried out. The LSVs of pure RMC and Tyr-RMC were firstly recorded. As depicted in Fig. 2A, Tyr-RMC exhibited a larger photocurrent density compared with pure RMC under applied potentials from 0 to 0.4 V. Incidental photon-to-electron conversion efficiency (IPCE) spectroscopy is another fundamental tool to investigate the photoelectric behavior of photoactive materials. As Fig. 2B illustrates, by measuring the IPCE values at various wavelengths, the corresponding outcomes were obtained according to eqn (1)[25] with no bias voltage:

$$\mathrm{IPEC}\% = \frac{1240 \times j}{\lambda \times P} \times 100\% \quad (1)$$

where λ is the wavelength (nm), j is the short circuit photocurrent density (mA cm^{-2}), and P is the incident light power (mW cm^{-2}). Apparently, the Tyr-RMC complex presented a higher IPCE value and improved photoresponse in both the ultraviolet region and

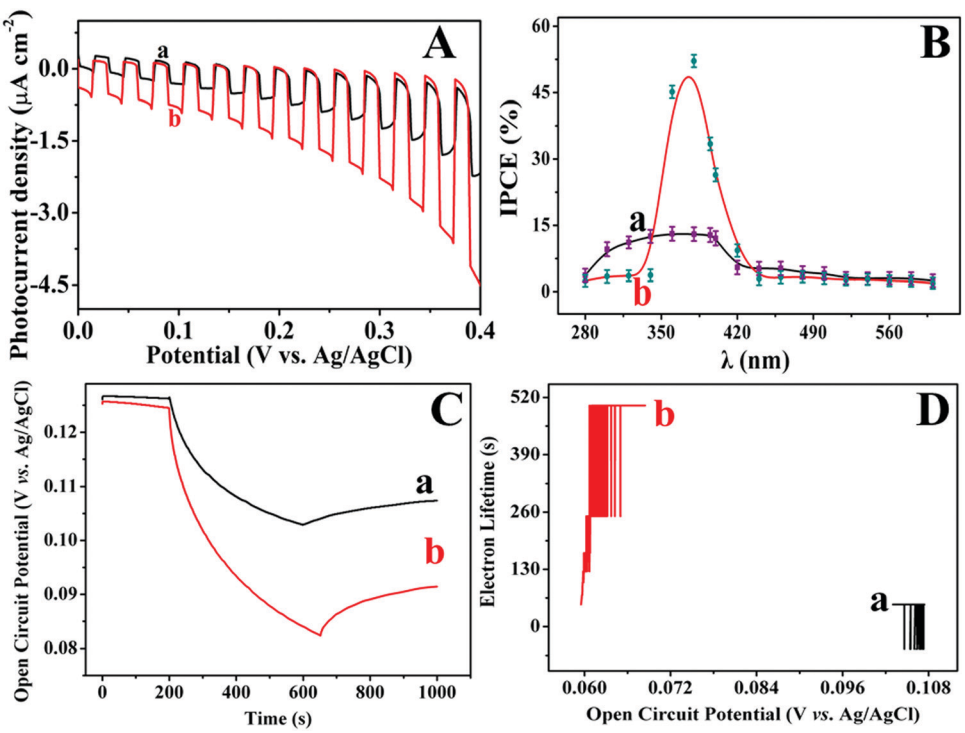

Fig. 2 (A) Applied potential bias-dependent photocurrent, (B) IPCE spectra, (C) open-circuit voltage response densities and (D) electron lifetimes of (a) RMC and (b) Tyr-RMC in PBS (pH 7.0) with an applied potential of 0.2 V.

visible light region. Subsequently, open-circuit voltage-decay measurements were conducted to investigate the recombination kinetics of the structure. As displayed in Fig. 2C, upon light illumination, abundant photoelectrons were excited from the photoactive materials and accumulated on the electrode interface, thereby causing more negative potential of the Fermi level and increasing the V_{oc} value.[31] However, once the irradiation stopped, the V_{oc} decayed gradually due to recombination of photogenerated electron–hole pairs and scavenging of accumulated photoelectrons by the electron acceptor species in solution. As expected, Tyr-RMC exhibited a higher V_{oc} value than pure RMC under light illumination and slower decay in the dark, implying that Tyr-RMC possesses more efficient charge separation and a lower charge recombination rate. Subsequently, the electron lifetimes of the photoactive materials were calculated according to eqn (2):[26]

$$\tau = \frac{k_B T}{e}\left(\frac{dV_{OC}}{dt}\right)^{-1} \quad (2)$$

where τ, e, and k_B are the potential dependent lifetime, charge of a single electron, and Boltzmann's constant, respectively, T is the temperature, and dV_{oc}/dt is the derivative of the transient open-circuit voltage. Accordingly, we can infer that the lifetime of the electrons mainly depends on dV_{oc}/dt. Obviously, as depicted in Fig. 2D, Tyr-RMC exhibited a longer decay lifetime of accumulated electrons because of its slower decay of the V_{oc} value in the dark compared to pure RMC. The results discussed above strongly confirm that tyramine greatly improved the PEC performance of RMC for self-oxidation of tyramine and hindered the recombination of electron–hole pairs, thereby triggering more efficient electron transmission.

3.3 Characterization of the PEC biosensor

To verify the successful construction process of the PEC biosensor, electrochemical impedance spectroscopy (EIS) at various assembly stages was performed to characterize the stepwise modification of the electrode. As shown in Fig. 3A, the bare GCE exhibited a small electron transfer resistance (curve a), indicating that a clean GCE was obtained. When the CNHs (curve b) attached to the electrode, the resistance decreased because of their outstanding conductivity. Also, when the Au NCs (curve c) were coated onto the electrode, the resistance decreased significantly because the Au NCs are conductive to the transmission of electrons. However, as poly(Gly) and ZEN antibody were successively modified (curves d and e) on the electrode, the resistance increased gradually because the poor conductivity of poly(Gly) and the insulating properties of ZEN antibody hindered the electron transmission. After a competitive reaction took place between peptide@Tyr-RMC conjugate and free target ZEN, the resistance was further enhanced, suggesting that peptide@Tyr-RMC was successfully captured onto the electrode surface *via* specific recognition reactions (curve f). Furthermore, dramatically increased resistance was observed when treating the resulting electrode with HRP–H_2O_2 (curve g). The reason may be that deposition of tyramine caused rolling circle extension of the Tyr-RMC chain which, with the accumulation of RMC, persistently enhanced the steric hindrance and severely blocked the electronic transmission channels.

In addition, the photocurrent responses of the electrodes after each modification step were investigated. As depicted in Fig. 3B, under illumination, the photocurrent response on the electrode interface was ignorable at the beginning (curves a to e) until the peptide@Tyr-RMC conjugate was anchored on the electrode *via* a competitive reaction (curve f); then, the photocurrent remarkably increased. It is known that RMC as a superior photoactive material loses electrons under illumination and transfers them rapidly to the photoelectrode with the assistance of CNHs and Au NCs (see Scheme 2). The mechanism can be described as follows: first, self-oxidation of tyramine suppressed the electron–hole recombination and prolonged the lifetime of the electron–hole pairs. For another, the Schottky barrier between the CNHs and Au NCs drove the photogenerated electrons and holes in different directions, which favored more efficient charge separation in the RMC.[21,22] Moreover, it is worth mentioning that the localized surface plasmonic resonance (LSPR) effect enhanced the incident light absorption ability of the Au NCs, forcing a collective oscillation of electrons. As a result, large

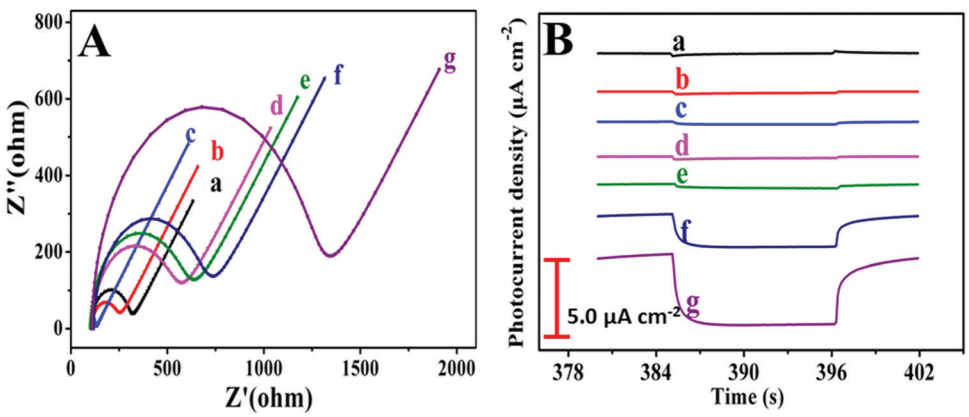

Fig. 3 (A) EIS and (B) photocurrent density measurements on different modified electrodes: (a) bare GCE, (b) GCE/CNHs, (c) GCE/CNHs/Au NCs, (d) GCE/CNHs/Au NCs/poly(Gly), (e) GCE/CNHs/Au NCs/poly(Gly)/Ab, (f) GCE/CNH/Au NCs/poly(Gly)/Ab/peptide@Tyr-RMC, (g) GCE/CNH/Au NCs/poly(Gly)/Ab/peptide@Tyr-RMC/HRP–H_2O_2. All of the photocurrent responses were recorded in PBS (pH 7.0) at an applied potential of 0.2 V, and the electrochemical impedance was determined in a mixed solution of 5.0 mM $K_3[Fe(CN)_6]/K_4[Fe(CN)_6]$ (1 : 1) containing 0.5 M KCl with an applied potential of 0.199 V.

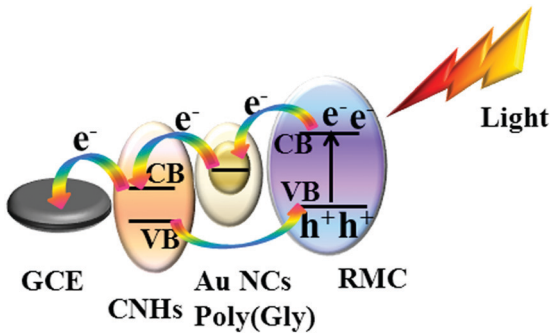

Scheme 2 Photocurrent generation mechanism of the PEC biosensor.

amounts of electrons and holes were excited to generate more brilliant photocurrent response on the electrode interface.[27,28] After catalysis by HRP–H_2O_2 (curve g), tyramine was deposited at the site of the enzyme reaction, causing localized accumulation of Tyr-RMC. As expected, benefiting from the outstanding PEC properties of RMC and the powerful rolling circle amplification effect of the RMC-TSA strategy, a sharp increase of the photocurrent was displayed. These results preliminarily confirm the successful construction of the biosensor and its feasibility as a target ZEN monitor.

3.4 Optimization of conditions for detection

In order to obtain optimal immunoassay performance, several parameters were investigated during the fabricating and detecting processes. The best results are exhibited in Fig. S6 and S7 (ESI†). As presented in Fig. S6A (ESI†), the optional volume ratio between Au NCs and MEA was 1 : 3. As displayed in Fig. S6B (ESI†), after 25 cycles of cyclic voltammetry, the Gly was electrodeposited on the electrode interface, and the maximum peak of the photocurrent appeared. Also, the optimal concentration of RMC was 3 mg mL^{-1} (Fig. S6C, ESI†). Additionally, Fig. S7A (ESI†) indicates that 30 min was the optimal absorption time between RMC and tyramine. Fig. S7B (ESI†) illustrates that the optimal incubation time of ZEN antibody was 50 min. Also, the optional competitive reaction time between target free ZEN and peptide@Tyr-RMC conjugate was 30 min (Fig. S7C, ESI†). Moreover, the catalysis time of HRP–H_2O_2 on the electrode interface was also evaluated, and the optimal result appeared to be 15 min (Fig. S7D, ESI†). Furthermore, pH and applied potential have critical effects during the detecting processes; the pH of the PBS solution used in the PEC measurements was 7.0 (Fig. S7E, ESI†), and the applied potential for the PEC measurements was 0.2 V (Fig. S7F, ESI†).

3.5 Analytical performance of the dual-signal readout biosensor

Under optimum conditions, the photocurrent–time curves in Fig. 4A indicate rapid photocurrent response to different ZEN concentrations. The photocurrent gradually decreased with increasing concentration of ZEN (a–g) because less peptide@Tyr-RMC conjugate could be captured onto the electrode *via*

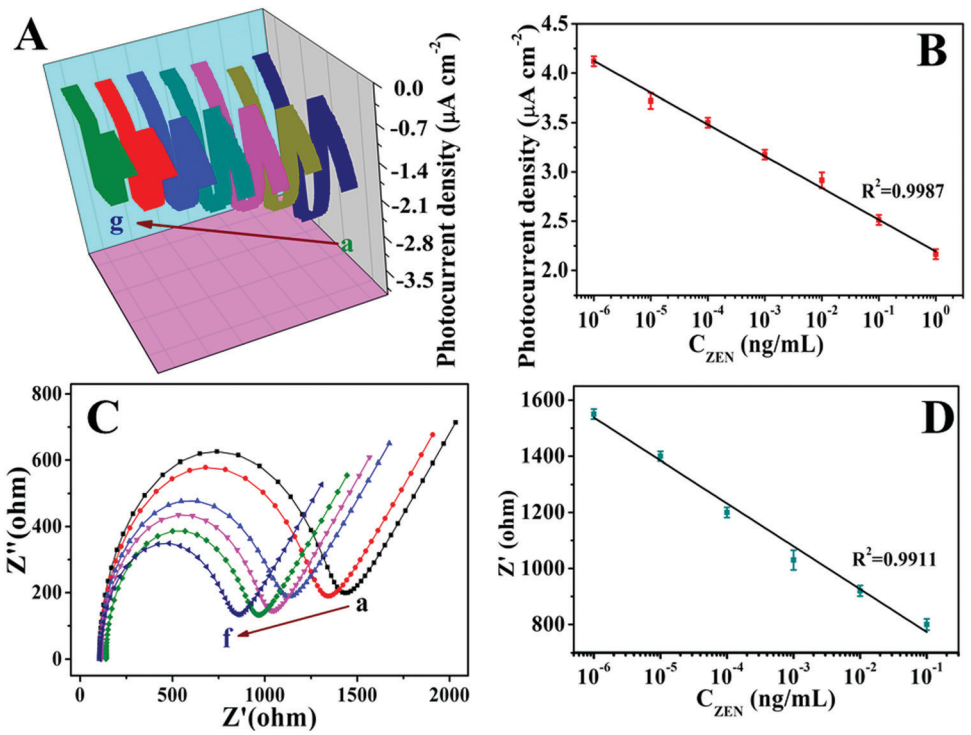

Fig. 4 (A) The photocurrent density responses and (B) the corresponding calibration curves for different concentrations (a–g) of the photocurrent density to ZEN after treatment with 0.5 mg mL^{-1} HRP. (C) EIS and (D) the corresponding calibration curves for different concentrations (a–f) of ZEN based on the electrochemical impedance after treatment with 0.5 mg mL^{-1} HRP–H_2O_2. All the photocurrent responses were recorded in PBS (pH 7.0) at an applied potential of 0.2 V, and the electrochemical impedance was determined in a mixed solution of 5.0 mM $K_3[Fe(CN)_6]/K_4[Fe(CN)_6]$ (1 : 1) containing 0.5 M KCl with an applied potential of 0.199 V.

Table 1 Comparison of various methods of ZEN detection

Detection methods	Linear range	LOD	Ref.
Fluoroimmunoassay	0.038 to 0.977 ng mL^{-1}	0.012 ng mL^{-1}	9
Immunochromatographic assay	0.1 to 10 ng mL^{-1}	0.0591 ng mL^{-1}	8
Fluorescent ELISA	0.0024 to 1.25 ng mL^{-1}	0.075 ng mL^{-1}	6
Fluorescence aptasensor sensor	0.05 to 100 ng mL^{-1}	0.007 ng mL^{-1}	7
Amperometric ELISA	0.005 to 15 ng mL^{-1}	0.0017 ng mL^{-1}	29
Cell electrochemical impedance	0.1 to 50 μg mL^{-1}	50 ng mL^{-1}	30
FRET ELISA	1 to 10 ng mL^{-1}	0.09 ng mL^{-1}	42
UV-induced fluorescence immunoassay	1.0 to 1000 ng mL^{-1}	0.21 ng mL^{-1}	43
Dual-signal readout C-ELISA	10^{-6} to 10 ng mL^{-1}	1×10^{-6} ng mL^{-1}	This work

competitive reactions. Fig. 4B presents the linear relationship between the ZEN concentration (C_{ZEN}) and photocurrent density; the linear regression equation can be expressed as photocurrent density (μA cm^{-2}) = $-0.318 \log C_{ZEN}$ (ng mL^{-1}) + 1.99 (R^2 = 0.9987) with a linear range of 10^{-6} ng mL^{-1} to 1 ng mL^{-1}, where $\log C_{ZEN}$ is the logarithm of the ZEN concentration. Additionally, in Fig. 4C, it is interesting to find that the electrochemical impedance response is also related to the concentration of ZEN (a–f). Accordingly, as Fig. 4D exhibits, the electrochemical impedance in the sensing interface gradually decreased with increasing C_{ZEN}; the linear regression equation can be expressed as Z' (Ohm) = $-152.93 \log C_{ZEN}$ (ng mL^{-1}) + 620.30 (R^2 = 0.9911) in a linear range between 10^{-6} ng mL^{-1} and 10^{-1} ng mL^{-1}. The standard curves presented above were fitted from the S-shaped curves in Fig. S3A and B (ESI†) and calibrated *via* the % bias plots in Fig. S3C and D (ESI†);[35] the detection limit in this work was calculated to be 10^{-6} ng mL^{-1}. Due to the brilliant signal amplification effect of Tyr-RMC, the dual-signal readout competitive enzyme-linked immunoassay (C-ELISA) exhibited a wider linear range and lower detection limit compared to other more conventional ELISAs (Table 1).

3.6 Specificity, reproducibility, and stability of the dual-signal readout biosensor

The selectivity of the dual-signal readout immunoassay was tested against two other mycotoxins, aflatoxin B1 (AFB1) and vomitoxin (DON), at hundredfold excess concentrations. As illustrated in Fig. 5A, the photocurrent responses toward non-target ZEN samples, including AFB_1 (a), DON (b), AFB1 and DON (c), were much

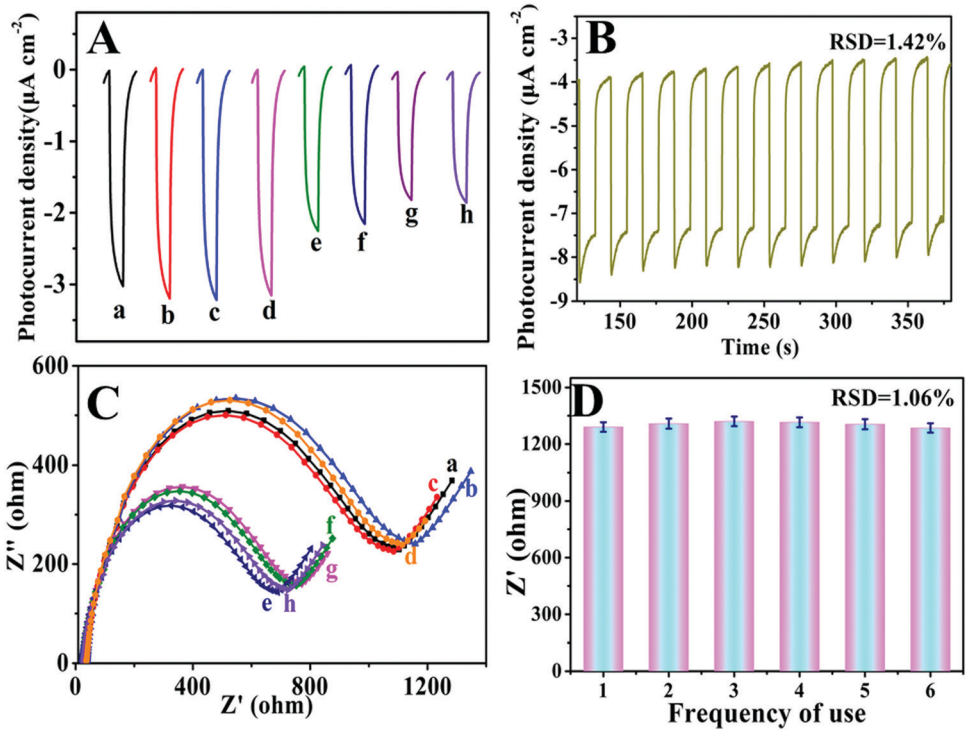

Fig. 5 (A) and (C) Selectivity of the proposed assay towards photocurrent density and EIS determined by comparing with interfering substances at the 0.1 ng mL^{-1} level: AFB_1 (a), DON (b), AFB_1 + DON (c), blank (d), 0.001 ng mL^{-1} ZEN + AFB_1 (e), 0.001 ng mL^{-1} ZEN + DON (f), AFB_1 + DON (g), and AFB_1 + DON + ZEN (h) in 0.1 M PBS. (B) The repeatability test for the response of the GCE/CNH/Au NCs/poly(Gly)/Ab/peptide@Tyr-RMC/HRP electrode to time-based photocurrent density with a light switched on and off. (D) The repeatability test for the response of the GCE/CNH/Au NCs/poly(Gly)/Ab/peptide@Tyr-RMC/HRP–H_2O_2 electrode to electrochemical impedance. All of the photocurrent responses were recorded in PBS (pH 7.0) at an applied potential of 0.2 V, and the electrochemical impedance was determined in a mixed solution of 5.0 mM $K_3[Fe(CN)_6]/K_4[Fe(CN)_6]$ (1 : 1) containing 0.5 M KCl with an applied potential of 0.199 V.

higher than those in the presence of ZEN (ZEN + AFB_1 (e), ZEN + DON (f), ZEN (g), Mix (h)) and did not show significant changes compared to that of the blank control (d). Concretely, in the presence of ZEN (e–h), no obvious difference was observed between ZEN + AFB_1 (e) and ZEN (g). However, when ZEN was mixed with DON (ZEN + DON (f) and AFB1 + DON + ZEN (h)), a slightly decreased photocurrent response emerged. The reason is that DON took up some of the combine sites *via* non-specific recognition, which further inhibited the photocurrent output, resulting in decreased signal response.[40,41] Similarly, as revealed in Fig. 5C, the electrochemical impedance toward AFB_1 (a), DON (b), AFB1 and DON (c) and blank (d) was stronger than that in the presence of the target ZEN (e–h). Meanwhile, when ZEN was mixed with DON (f and h), the electrochemical impedance further declined, which was consistent with the results in Fig. 5A. Moreover, the competitive inhibition curves of ZEN, AFB1 and DON were established in Fig. S4 (ESI†) to further illustrate the specificity of the designed dual-signal readout biosensor. The results in Fig. S4 (ESI†) present that the half maximal (50%) inhibitory concentration (IC50) of ZEN was calculated to be 0.0144 ng mL^{-1}. Also, the IC50 values of AFB1 and DON were both greater than the highest concentration in the standard curve (1 ng mL^{-1}). Therefore, the discussion above verifies that this PEC immune biosensor possesses acceptable specificity in the linear range from 10^{-6} ng mL^{-1} to 1 ng mL^{-1}. Fig. 5B shows the stability of the photocurrent response of the GCE/CNH/Au NCs/poly(Gly)/Ab/peptide@Tyr-RMC/HRP–H_2O_2 electrode; the photocurrent response showed no noticeable changes under several on/off irradiation cycles, with a relative standard deviation (RSD) of 1.42%. In addition, the Z' value in the GCE/CNH/Au NCs/poly(Gly)/Ab/peptide@Tyr-RMC/HRP–H_2O_2 electrode remained stable with increasing frequency of use; as shown in Fig. 5D, the RSD was 1.06%, which implies that the designed sensing platform possesses satisfactory stability. It is known that reproducibility is a key point in an ultrasensitive assay. Thus, reproducibility tests for both the photocurrent response and electrochemical impedance were performed in four electrodes (GCE/CNH/Au NCs/poly(Gly)/Ab/peptide@Tyr-RMC/HRP–H_2O_2). As illustrated in Fig. S5A (ESI†), the RSDs of the four experiments for the photocurrent response test were 2.68%, 3.64%, 1.77% and 2.86%, respectively. Also, in Fig. S5B (ESI†), the Z' values in the corresponding four electrodes were 1303.25, 1311.25, 1320.5 and 1378.25, respectively, showing outstanding reproducibility of the designed biosensor. Finally, to examine the performance of the proposed dual-signal readout sensing platform in practical applications, the biosensor was applied to soybean sauce samples spiked with 0.1, 0.01 and 0.001 ng mL^{-1} ZEN. The recoveries of the added ZEN ranged from 99.3% to 105.1% (Table S1, ESI†), implying that this PEC biosensor possessed acceptable precision and can be widely applied in monitoring ZEN in actual samples.

4. Conclusions

In summary, a superior non-toxic dual-signal readout sensing platform was constructed and realized ultrasensitive detection of ZEN. A valid peptide@Tyr-RMC probe was successfully fabricated by selecting a mimotope peptide from a phage-displayed library and labeling it with Tyr-RMC composite. The mimotope peptide could be utilized as a mimic of ZEN, which avoided using mycotoxin itself and decreased damage to both the operator and environment. Subject to catalysis of HRP–H_2O_2, the Tyr-RMC composite was deposited at the site of the enzyme reaction. Also, as the report units in the probe, the localized accumulation of the Tyr-RMC composite led to rolling circle amplification of both the photocurrent response and electrochemical impedance, which efficiently promoted the sensitivity and precision during the measurement. This well-designed immunoassay provides a reliable method for rapid and sensitive ZEN detection in a wide linear range with a low detection limit. The successful demonstration of this approach indicates that it holds great potential in practical applications of food safety testing.

Conflicts of interest

There are no conflicts to declare.

Acknowledgements

This project was financially supported by the NSFC (21877012, 21575024) and the National Science Foundation of Fujian Province (2016J06003, 2017J01620); the Education Department of Fujian Province (JK2016009, FBJG20170186, JA14071) is also greatly acknowledged.

References

1 M. Hervás, M. A. López and A. Escarpa, *Biosens. Bioelectron.*, 2010, **25**, 1755.
2 S. C. Pei, W. J. Lee, G. P. Zhang, X. F. Hu, S. A. Eremin and L. J. Zhang, *Food Control*, 2013, **31**, 65.
3 M. Regiart, O. Fernández, A. Vicario, J. Villarroel-Rocha, K. Sapag, G. A. Messina, J. Raba and F. A. Bertolino, *Microchem. J.*, 2018, **141**, 388.
4 A. B. Serrano, G. Font, J. Maes and E. Ferrer, *Food Anal. Methods*, 2016, **9**, 856.
5 H. L. Zheng, H. Yi, W. Lin, H. Dai, Z. S. Hong, Y. Y. Lin and X. H. Li, *Electrochim. Acta*, 2018, **260**, 847.
6 S. N. Zhan, X. L. Huang, R. Chen, J. Li and Y. H. Xiong, *Talanta*, 2016, **158**, 51.
7 Z. Z. Wu, E. B. Xu, F. J. Chughtai, Z. Y. Jin and J. Irudayaraj, *Food Chem.*, 2017, **230**, 673.
8 Y. N. Shao, H. Duan, L. Guo, Y. K. Leng, W. H. Lai and Y. H. Xiong, *Anal. Chim. Acta*, 2018, **1025**, 163.
9 F. Y. Zhang, B. Liu, W. Sheng, Y. Zhang, Q. Liu, S. J. Li and S. Wang, *Food Chem.*, 2018, **225**, 421.
10 Q. H. He, Y. Xu, Y. H. Huang, R. R. Liu, Z. B. Huang and Y. P. Li, *Food Chem.*, 2011, **126**, 1312.
11 A. Rami, M. Behdani, N. Yardehnavi, M. Habibi-Anbouhi and F. Kazemi-Lomedasht, *Asian Pac. J. Trop. Biomed.*, 2017, **7**, 599.

12 R. Jahdasani, F. R. Jamnani, M. Behdani, M. Habibi-Anbouhi, N. Yardehnavi and D. Shahbazzadeh, *Toxicon*, 2016, **124**, 83.
13 D. Ando, M. Inoue, H. Kamada, S. Taki, T. Furuya, Y. Abe, K. Nagano, Y. Tsutsumi and S. J. Tsunoda, *Biochem. Biophys. Rep.*, 2016, **7**, 309.
14 T. B. Lan, T. Wang, W. F. Zhang, N. L. Wu and M. D. Wei, *J. Alloys Compd.*, 2017, **699**, 455.
15 P. S. Liu, W. P. Cai, L. X. Wang, M. D. Shi, X. D. Luo and W. P. Jing, *Trans. Nonferrous Met. Soc. China*, 2009, **19**, 743.
16 X. Zhou, Y. Li, H. Wu, W. Huang, H. Ju and S. Ding, *Biosens. Bioelectron.*, 2019, **130**, 88.
17 P. Liu, C. Li, R. Zhang, Q. Tang, J. Wei, Y. Lu and P. Shen, *Biosens. Bioelectron.*, 2019, **126**, 543.
18 L. Hou, Y. Tang, M. Xu, Z. Q. Gao and D. P. Tang, *Anal. Chem.*, 2014, **86**, 8352.
19 J. Zhou, J. Tang, G. N. Chen and D. P. Tang, *Biosens. Bioelectron.*, 2014, **54**, 323.
20 R. N. Ma, L. L. Wang, M. Zhang, L. P. Jia, W. Zhang, L. Shang, W. L. Jia and H. S. Wang, *Sens. Actuators, B*, 2018, **257**, 678.
21 M. Kumar, V. S. Bhati and M. Kumar, *Int. J. Hydrogen Energy*, 2017, **42**, 22082.
22 H. Dai, S. P. Zhang, Y. L. Li and Y. Y. Lin, *Analyst*, 2015, **140**, 3514.
23 Z. S. Hong, K. Q. Zhou, J. W. Zhang, Z. G. Huang and M. D. Wei, *J. Mater. Chem. A*, 2015, **3**, 17412.
24 Y. Y. Li, X. M. Ma, Z. M. Xu, M. H. Liu, Z. Y. Lin, B. Qiu, L. H. Guo and G. N. Chen, *Analyst*, 2016, **141**, 2970.
25 A. Kongkanand, K. Tvrdy, K. Takechi, M. Kuno and P. V. Kamat, *J. Am. Chem. Soc.*, 2008, **130**, 4007.
26 J. Bisquert, A. Zaban, M. Greenshtein and I. Mora-Sero, *J. Am. Chem. Soc.*, 2004, **126**, 13550.
27 Y. H. Lee, D. H. Kim and T. W. Kim, *Appl. Surf. Sci.*, 2015, **355**, 359.
28 H. T. Chou, W. H. Huang, T. M. Wu, Y. K. Yu and H. C. Hsu, *Sens. Bio Sensing Res.*, 2017, **14**, 17.
29 L. Liu, Y. J. Chao, W. Cao, Y. L. Wang, C. N. Luo, X. H. Pang, D. W. Fan and Q. Wei, *Anal. Chim. Acta*, 2014, **847**, 29.
30 W. S. Gu, P. Zhu, D. L. Jiang, X. X. He, Y. Li, J. Ji, L. J. Zhang, Y. G. Sun and X. L. Sun, *Biosens. Bioelectron.*, 2015, **70**, 447.
31 Y. L. Zhou, M. Wang, Z. Q. Yang, H. S. Yin and S. Y. Ai, *Sens. Actuators, B*, 2015, **206**, 728.
32 L. Lv, K. Li, Y. Xie, Y. Cao and X. Zheng, *Mater. Sci. Eng., C*, 2017, **78**, 96.
33 J. M. Peng, Y. L. Su, W. J. Chen, X. T. Zhao, Z. G. Jiang, Y. N. Dong, Y. Zhang, J. Z. Liu and X. Z. Cao, *J. Membr. Sci.*, 2013, **427**, 92.
34 K. X. Ren, C. L. He, Y. L. Cheng, L. Gao and X. S. Chen, *Polym. Chem.*, 2014, **5**, 5069.
35 M. Azadeh, B. Gorovits, J. Kamerud, S. MacMannis, A. Safavi, J. Sailstad and P. Sondag, *AAPS J.*, 2018, **20**, 22.
36 M. Kurisawa, J. E. Chung, Y. Y. Yang, S. J. Gao and H. Uyama, *Chem. Commun.*, 2005, 4312.
37 Z. P. Zeng, Y. Q. She, Z. P. Peng, J. C. Wei and X. H. He, *RSC Adv.*, 2016, **6**, 8032.
38 B. Bi, H. Liu, W. Kang, R. Zhuo and X. Jiang, *Colloids Surf., B*, 2019, **175**, 614.
39 K. V. Harisha, B. E. Kumara Swamy and E. E. Ebenso, *J. Electroanal. Chem.*, 2018, **823**, 730.
40 S. C. Pei, W. J. Lee, G. P. Zhang, X. F. Hu, S. A. Eremin and L. J. Zhang, *Food Control*, 2013, **31**, 65.
41 W. S. Gu, P. Zhu, D. L. Jiang, X. X. He, Y. Li, J. Ji, L. J. Zhang, Y. G. Sun and X. L. Sun, *Biosens. Bioelectron.*, 2015, **70**, 447.
42 T. Li, J. Y. Byun, B. B. Kim, Y. B. Shin and M. G. Kim, *Biosens. Bioelectron.*, 2013, **42**, 403.
43 Q. Shu, Y. Wu, L. Wang and Z. Fu, *Talanta*, 2019, **204**, 261.

